

Soil-water-air Coupled Finite Element Analysis on Slope Failure in Unsaturated Soil

Y.L. Xiong¹, X.H. Bao² and F. Zhang¹

¹ Department of Civil Engineering, Nagoya Institute of Technology, Nagoya, Japan

² Department of Civil Engineering, Shenzhen University, Shenzhen, China

E-mail: cho.ho@nitech.ac.jp

ABSTRACT: In this paper, a program of finite element method named as SOFT, using finite element-finite difference scheme (FE-FD) in soil-water-air three-phase coupling problem has been developed based on a rational constitutive model for unsaturated soil proposed by Zhang and Ikariya (2011), which can properly take into consideration of moisture characteristics of unsaturated soils. In the program, the FE-FD formulation in saturated condition proposed by Oka *et al.* (1994) has been extended to unsaturated condition. In order to verify the availability of the program, a model test on slope failure of unsaturated soil, carried out by Kitamura *et al.* (2007), is simulated by the proposed numerical method. From the results, it is known that the test results can be described in a satisfactory accuracy on the whole.

1. INTRODUCTION

A lot of slope failures due to rainfall were reported each year in Japan, especially in rainy season. Among these, underground water table was usually below the ground surface and the pore water pressures in the soil above the underground water table are negative. This negative pore water pressure, referred to as suction that will contribute to the stability of unsaturated soil slopes. With the infiltration of water in the rainy season, water seepage can cause a gradual loss of suction in an unsaturated soil slope with the increase of saturation. The loss of suction furthermore causes a decrease in effective stress and consequently a decrease of shear strength of the soil, sometime may even cause slope failure.

In order to investigate the mechanism of slope failure, some experiments on slope failure due to rainfall have been done in the lab such as Kitamura *et al.* (2007), Yagi *et al.* (1983) and Tohari *et al.* (2007). In the work by Kitamura *et al.*, several patterns of the model tests were conducted on different conditions such as position of water injection, rain intensity, inclined degree of slope, etc. In this paper, a FE-FD program, named as soft, based on an elastoplastic constitutive model for unsaturated soil proposed by Zhang and Ikariya (2011), is used to simulate the aforementioned model test in order to verify the availability of the proposed numerical method.

2. FE-FD MATHEMATICAL FORMULATION

The governing equations soil-water-air three-phase coupling problem can be classified into three groups: equilibrium equation, continuity equation of water and continuity equation of air. The detailed derivation of soil-water two-phase equations can be referred to the work by Oka *et al.* (1994). While the soil-water-air three-phase equations can be referred to the work by Uzuoka *et al.* (2007 and 2008), Uzuoka (2010), Li *et al.* (2004) and Borja (2005). Here these equations are directly written in the following:

I. Equilibrium equation

$$\frac{\partial \sigma_{ij}}{\partial x_j} + \rho b_i = 0 \quad (1)$$

II. Continuity equation of water

$$\frac{\dot{\epsilon}_{ii}^s}{n} - \frac{k^w}{\gamma^w} \frac{\partial^2 p^w}{\partial x_i \partial x_i} - \frac{1}{K^w} \dot{p}^w + \frac{\dot{S}_r}{S_r} = 0 \quad (2)$$

III. Continuity equation of air

$$\frac{\dot{\epsilon}_{ii}^s}{n} - \frac{k^a}{\gamma^a} \frac{\partial^2 p^a}{\partial x_i \partial x_i} - \frac{1}{K^a} \dot{p}^a - \frac{\dot{S}_r}{1-S_r} = 0 \quad (3)$$

Where b_i is body force, S_r is degree of saturation, K is the volumetric elastic coefficient, k is permeability, p is fluid pressure, n

is porosity, and the superscript of s , w and a in the above equation denotes the solid, water and air phase respectively.

For simplicity, it is assumed that the air in the soil is always connecting to atmosphere and its value is given as 0 in this paper, therefore the continuity equation of air can be satisfied automatically.

2.1 Discretization of equilibrium equation

By using virtual work theorem, the weak form of the equilibrium equation in an arbitrary region v can be expressed as following

$$\int_v \left(\frac{\partial \sigma_{ij}}{\partial x_j} + \rho b_i \right) \delta u_i^s dV = 0 \quad (4)$$

where, δu_i^s is the arbitrary virtual displacement.

Based on Gaussian's theory and boundary condition, Equation (4) can be changed as

$$\int_v \sigma_{ij} \delta \epsilon_{ij}^s dV = \int_v \rho b_i \delta u_i^s dV + \int_s T_i \delta u_i^s dS \quad (5)$$

where, T_i is surface force, $\delta \epsilon_{ij}^s$ is the arbitrary virtual strain.

The effective stress for unsaturated soil is expressed as,

$$\sigma_{ij} = \sigma_{ij}^i + S_r p^w + (1 - S_r) p^a = \sigma_{ij}^i + S_r p^w \quad (6)$$

Substituting Equation (6) into Equation (5), the following equation can be obtained

$$\int_v (\sigma_{ij}^i + S_r p^w) \delta \epsilon_{ij}^s dV = \int_v \rho b_i \delta u_i^s dV + \int_s \Delta T_i \delta u_i^s dS \quad (7)$$

The incremental form of the above equation in finite element scheme can be written as follow:

$$\begin{aligned} & \int_v \Delta \sigma_{ij}^i \delta \epsilon_{ij}^s dV + \int_v \Delta (S_r p^w) \delta \epsilon_{ii}^s dV \\ & = \int_v \rho \Delta b_i \delta u_i^s dV + \int_s \Delta T_i \delta u_i^s dS \end{aligned} \quad (8)$$

In the proposed program, we use different shape function for displacement and pore water pressure in one element. The variables of displacement are given at the nodes and the variables of pore water pressure are given at the gravitational center.

For one element, \vec{u}_N is denoted as the displacement vector of all nodes, and p_{dE} is denoted as the excessive pore water pressure at gravitational center. The displacement vector of any arbitrary point within this element, \vec{u}^s can be expressed by the displacement vector of nodes \vec{u}_N

$$\bar{u}^s = [N] \bar{u}_N, \quad \delta \bar{u}^s = [N] \delta \bar{u}_N \quad (9) \quad \Delta S_r = k_s^{-1} \Delta s \quad (21)$$

Here, $[N]$ is shape function matrix. The strain vector of any arbitrary point within an element can be written as,

$$\bar{\epsilon}^s = [L] \bar{u}^s = [L][N] \bar{u}_N = [B] \bar{u}_N \quad (10)$$

$$\delta \epsilon_{ii}^s = \delta \epsilon_v^s = [M][L][N] \delta \bar{u}_N = \bar{B}_v^T \delta \bar{u}_N = \delta \bar{u}_N^T \bar{B}_v \quad (11)$$

where, $[M] = \begin{bmatrix} 1 & 0 & 0 & 0_{3 \times 3} \\ 0 & 1 & 0 & 0_{3 \times 3} \\ 0 & 0 & 1 & 0_{3 \times 3} \\ 0_{3 \times d} & 0_{3 \times d} & 0_{3 \times d} & 0_{3 \times 3} \end{bmatrix}$, $[B] = [B_1 \dots B_i \dots B_n]$

and $[L] = \begin{bmatrix} \partial/\partial x & 0 & 0 & \partial/\partial y & 0 & \partial/\partial z \\ 0 & \partial/\partial y & 0 & \partial/\partial x & \partial/\partial z & 0 \\ 0 & 0 & \partial/\partial z & 0 & \partial/\partial y & \partial/\partial x \end{bmatrix}$

On the one hand, the constitutive model used in the program with vector form can be written as,

$$\Delta \bar{\sigma} = [D]^e [B] \bar{u}_N - E^{RFS} \Delta S_r \quad (12)$$

where, $E^{RFS} = \frac{1}{C_p} \frac{Q}{1+e_0} \frac{1}{D} [D]^e \frac{\partial f}{\partial \sigma}$, $[D]^e$ and $[D]^p$ are the elastic matrix stiffness and elasto-plastic matrix stiffness respectively (Zhang and Ikariya, 2011).

Because the virtual displacement is arbitrary, by Equations (9), (10), (11) and (12), Equation (8) can be expressed with vector form as,

$$\int_V [B]^T [D]^p [B] dV \cdot \Delta \bar{u}_N - \int_V [B]^T \cdot E^{RFS} dV \cdot \Delta S_r + \int_V \bar{B}_v \Delta(S_r p_{dE}^w) dV = \int_V \rho [N]^T \Delta \bar{b} dV + \int_S [N]^T \Delta \bar{T} dS \quad (13)$$

By defining the following equations

$$\Delta \bar{F} = \int_V \rho [N]^T \Delta \bar{b} dV + \int_S [N]^T \Delta \bar{T} dS \quad (14)$$

$$[K] = \int_V [B]^T [D] [B] dV \quad (15)$$

$$\bar{K}_{Sat} = \int_V [B]^T \bar{E}^{RFS} dV \quad (16)$$

$$\bar{K}_v = \int_V \bar{B}_v dV \quad (17)$$

Equation (13) can be rewritten as,

$$[K] \Delta \bar{u}_N - \bar{K}_{Sat} \Delta S_r + \bar{K}_v \Delta(S_r p_{dE}^w) = \Delta \bar{F} \quad (18)$$

The incremental form of $\Delta(S_r p_{dE}^w)$ is approximated as,

$$\Delta(S_r p_{dE}^w) = \Delta S_r p_{dE}^w + S_r \Delta p_{dE}^w = \Delta S_{r|t+\Delta t} p_{dE|t}^w + S_{r|t} \Delta p_{dE|t+\Delta t}^w \quad (19)$$

$$\Delta S_{r|t+\Delta t} = S_{r|t+\Delta t} - S_{r|t} \quad (20)$$

On the other hand, in the work by Zhang and Ikariya (2011), a new moisture characteristics curve (MCC) is also proposed, where the relationship between the incremental suction and saturation is expressed as

where, k_s^{-1} is the stiffness of saturation-suction curve.

Substituting Equations (19) and (21) into Equation (18), we have,

$$[K] \Delta \bar{u}_N + \bar{K}_v S_r \Delta p_{dE}^w + (\bar{K}_v p_{dE}^w - \bar{K}_{Sat}) \cdot k_s^{-1} \cdot \Delta s = \Delta \bar{F} \quad (22)$$

The discretization of Equation (22) in time can be written as,

$$[K] \Delta \bar{u}_{N|t+\Delta t} + \bar{K}_v S_{r|t} \Delta p_{dE|t+\Delta t}^w + (\bar{K}_v p_{dE|t}^w - \bar{K}_{Sat}) k_s^{-1} \cdot \Delta s_{r|t+\Delta t} = \Delta \bar{F}_{r+\Delta t} \quad (23)$$

Because

$$\Delta s_{r|t+\Delta t} = s_{r|t+\Delta t} - s_{r|t} = (-p_{dE|t+\Delta t}^w) - (-p_{dE|t}^w) = p_{dE|t}^w - p_{dE|t+\Delta t}^w \quad (24)$$

Finally substituting Equation (24) into Equation (23), the discretization of equilibrium equation in space and time can be obtained,

$$[K] \Delta \bar{u}_{N|t+\Delta t} + \bar{F}_{Sat} p_{dE|t+\Delta t}^w = \Delta \bar{F}_{r+\Delta t} + \bar{F}_{Sat} p_{dE|t}^w \quad (25)$$

where, $\bar{F}_{Sat} = \bar{K}_v S_{r|t} - (\bar{K}_v p_{dE|t}^w - \bar{K}_{Sat}) \cdot k_s^{-1}$

2.2 Discretization of continuum equation

The discretization of continuity equation can be implemented by the same way and written as

$$\int_V \frac{\gamma^w}{k^w} S_r \bar{B}_v^T \bar{u}_N dV - \int_V \frac{\partial^2 p_{dE}^w}{\partial x_i \partial x_i} n S_r dV - \int_V \frac{\gamma^w}{k^w} \frac{n S_r}{K^w} \dot{p}_{dE}^w dV + \int_V \frac{\gamma^w}{k^w} n \dot{S}_r dV = 0 \quad (26)$$

As to continuity equation, a backward finite difference scheme (Akai and Tamura, 1978) is adopted for water flow. So the term of

$$\int_V \frac{\partial^2 p_{dE}^w}{\partial x_i \partial x_i} dV \text{ can be expressed as,}$$

$$\int_V \frac{\partial^2 p_{dE}^w}{\partial x_i \partial x_i} dV = \alpha p_{dE}^w - \sum_{i=1}^6 \alpha_i p_{dE}^w \quad (27)$$

where, $\alpha = \sum_{i=1}^4 \frac{S_i}{b_i}$, $\alpha_i = \frac{S_i}{b_i}$, S_i is center to center distance of an arbitrary element to its i^{th} neighboring element, b_i is drainage area of an arbitrary element in edge i .

By defining the following equations,

$$\int_V \frac{\gamma^w}{k^w} \cdot K^w dV \cdot \dot{p}_{dE}^w = \frac{\gamma^w}{k^w} \cdot \bar{V} \cdot \dot{p}_{dE}^w = A \cdot n \dot{p}_{dE}^w \quad (28)$$

$$\int_V \frac{\gamma^w n}{k^w} dV \cdot \dot{S}_r = \frac{\gamma^w n}{k^w} \cdot \bar{V} \cdot \dot{S}_r \quad (29)$$

Equation(26) can be rewritten as,

$$\frac{\gamma^w}{k^w} S_r \bar{K}_v^T \bar{u}_N - \alpha n S_r p_{dE}^w + \sum_{i=1}^6 \alpha_i n S_r p_{dE}^w - A n \dot{p}_{dE}^w + \frac{\gamma^w n}{k^w} \dot{S}_r \cdot \bar{V} = 0 \quad (30)$$

Because,

$$\begin{aligned} \bar{u}_{N|t+\Delta t} &= \frac{\Delta \bar{u}_{N|t+\Delta t}}{\Delta t}, \bar{p}_{dE|t+\Delta t} = \frac{p_{dE|t+\Delta t}^w - p_{dE|t}^w}{\Delta t} \\ \dot{S}_{r|t+\Delta t} &= \frac{S_{r|t+\Delta t} - S_{r|t}}{\Delta t} = \frac{\Delta S_{r|t+\Delta t}}{\Delta t} \end{aligned} \quad (31)$$

By substituting Equation (21), (24) and (31) into Equation (30), the continuity equation can be written as,

$$\begin{aligned} S_{rt} \bar{K}_v^T \cdot \Delta \bar{u}_{N|t+\Delta t} - \left[\frac{k^w \cdot \Delta t}{\gamma^w} \cdot n S_{rt} \alpha + \frac{k^w}{\gamma^w} \cdot (n S_{rt} A + \frac{\gamma^w}{k^w} n \bar{V} \cdot k_s^{-1}) \right] \\ \cdot p_{dE|t+\Delta t}^w - \sum_{i=1}^6 \frac{k^w \Delta t}{\gamma^w} n \alpha_i S_{rt} p_{idE|t+\Delta t}^w = - \frac{k^w}{\gamma^w} (A n S_{rt} + \frac{\gamma^w}{k^w} n \bar{V} \cdot k_s^{-1}) \cdot p_{dE|t}^w \end{aligned} \quad (32)$$

By defining the following equations,

$$\bar{\alpha} = \frac{n k^w \cdot \Delta t}{\gamma^w} \alpha \quad (33)$$

$$\bar{A} = \frac{n k^w}{\gamma^w} \cdot A \quad (34)$$

$$F_{sr} = n \bar{V} k_s^{-1} \quad (35)$$

$$\bar{\alpha}_i = \frac{n k^w \Delta t}{\gamma^w} \alpha_i \quad (36)$$

Finally, we can get the continuity equation discretized in space and time domains as,

$$\begin{aligned} S_{rt} \bar{K}_v^T \cdot \Delta \bar{u}_{N|t+\Delta t} - [(\bar{\alpha} + \bar{A}) S_{rt} + F_{sr}] \cdot p_{dE|t+\Delta t}^w \\ - \sum_{i=1}^6 \bar{\alpha}_i S_{rt} p_{idE|t+\Delta t}^w = -(\bar{A} S_{rt} + F_{sr}) \cdot p_{dE|t}^w \end{aligned} \quad (37)$$

By combining Equations (25) and (37), the FEM-FDM equations adopted in the program for static analysis can be finally written in the form as,

$$\begin{aligned} \left[\begin{array}{c} [K] \\ S_{rt} \bar{K}_v^T \end{array} \right] \left\{ \begin{array}{c} \bar{F}_{Sat} \\ -[(\bar{\alpha} + \bar{A}) S_{rt} + F_{sr}] \end{array} \right\} + \left\{ \begin{array}{c} 0 \\ \sum_{i=1}^m \bar{\alpha}_i S_{rt} p_{idE|t+\Delta t}^w \end{array} \right\} \\ = \left\{ \begin{array}{c} \Delta \bar{F}_{|t+\Delta t} + \bar{F}_{Sat} \cdot p_{dE|t}^w \\ -(\bar{A} S_{rt} + F_{sr}) \cdot p_{dE|t}^w \end{array} \right\} \end{aligned} \quad (38)$$

2.3 The performance of proposed program

Before simulating the model test by the proposed program, a simulation of one element is firstly done with two different loading conditions in order to verify the availability of the proposed program. The boundary conditions and loading conditions are shown in Figure 1. In Case 1, the element was firstly loaded to 0.4 MPa under constant suction (0.784 MPa) and then water injection (suction force decreased from -0.784 MPa to -0.392 MPa) was carried out under the condition that the total stress in y direction was kept constant (0.4MPa). In Case 2, a given displacement of 0.005m along y direction was firstly loaded under constant suction (0.784 MPa) and then water injection (suction force decreased from 0.784 MPa to 0.392 MPa) was carried out under the condition that the displacement loading is continued up to 0.01 m.

The moisture characteristics curve (MCC) is shown in Figure 2. Tables 1 and 2 show the parameters involved in the constitutive model and the corresponding MCC (Zhang and Ikariya, 2011). Detailed description of the physical meaning and the way of determination of these parameters can be referred to relevant reference (Zhang and Ikariya, 2011).

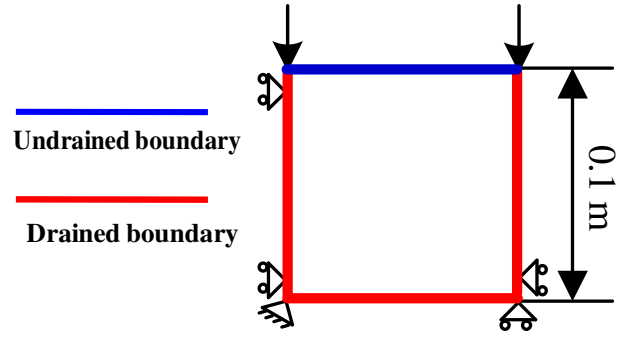


Figure 1 Boundary conditions of element simulation

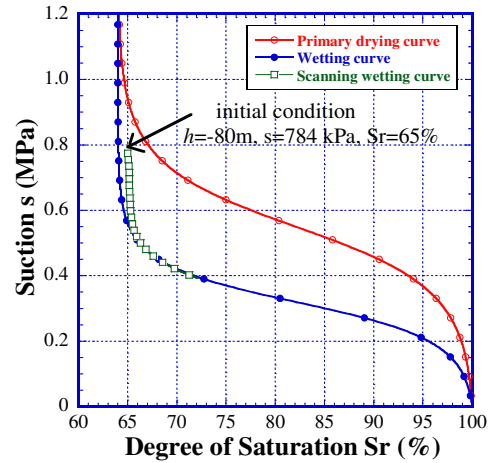


Figure 2 Simulated MCC for silty clay

Table 1 Material parameters of unsaturated silty clay

Compression index λ	0.050
Swelling index κ	0.010
Critical state parameter M	1.0
Void ratio N ($p'=98$ kPa on <i>N.C.L.</i>)	1.14
Poisson's ratio ν	0.30
Parameter of over consolidation a	5.00
Parameter of suction b	5.50
Parameter of over consolidation	1.0
Void ratio N_r ($p'=98$ kPa on <i>N.C.L.S.</i>)	1.38

Table 2 Parameters involved in MCC

Saturated degrees of saturation S_r^s	1.00
Residual degrees of saturation S_r^r	0.65
Parameter corresponding to drying AEV (kPa) S_d	550
Parameter corresponding to wetting AEV (kPa) S_w	320
Initial stiffness of scanning curve (kPa) k_{sp}^e	200000
Parameter of shape function c_1	0.008
Parameter of shape function c_2	0.013
Parameter of shape function c_3	10.0

Figure 3 shows the mechanical behaviours of unsaturated soil under aforementioned two loading condition. From the results, it is known that the collapse behaviour of unsaturated soil observed in the elementary test due to water injection (the decrease of suction) can be reproduced during the shear process, no matter what kind of

loading condition may be. In the figure, it is clear that when the suction reduced suddenly due to the water injection, the stress would also reduce significantly, showing a typical behaviour of the collapse.

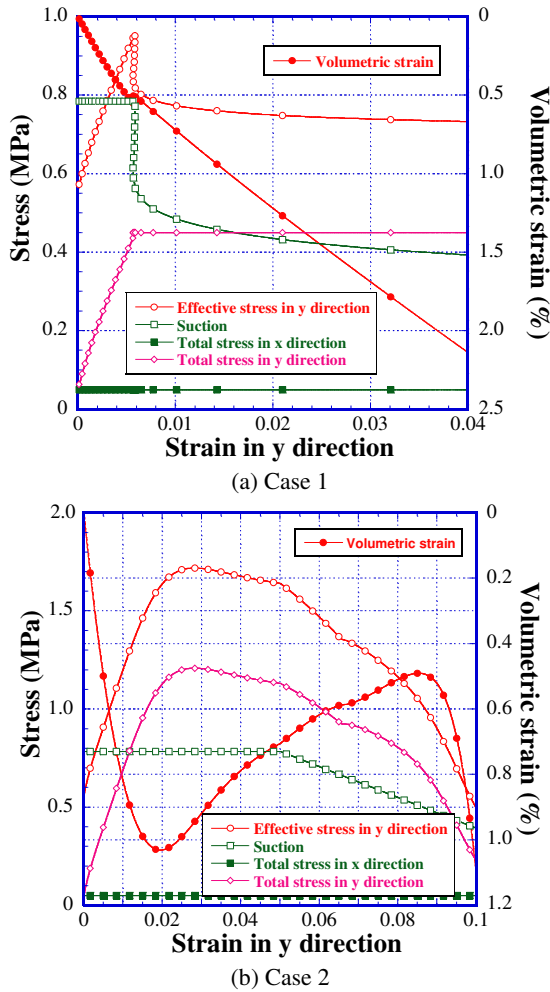


Figure 3 Mechanical behavior of unsaturated soil under two different loading conditions ($\sigma_{30} = 50$ kPa)

3. NUMERICAL SIMULATION OF MODEL TEST

Photo 1 shows the overall view of the experimental layout that is composed of a slope model made of compacted shirasu and some measuring devices. The slope model was compacted layer by layer carefully and each soil layer has a depth of 5 cm. The density of the soils listed in Table 3 was obtained by controlling the compaction numbers. The slope angle is 45° with the height of 80 cm. The permeable plates were used on the edges of the soil tank to control the boundary condition.

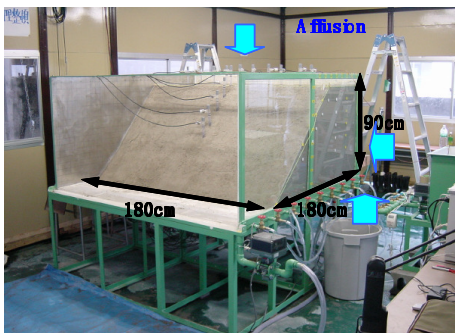


Photo 1 Whole view of soil tank testing apparatus, extracted from the work by Kitamura *et al.*, (2007)

The grain size distribution of Shirasu soil is shown in Figure 4. The density of Shirasu is 2.4 g/cm³, which is smaller than those of normal sandy soil. The physical properties of Shirasu are listed in Table 3.

Table 3 Physical properties of Shirasu

	Case 1	Case 2
Water content in nature (%)	25.6	23.3
Void ratio	1.57	1.47
Total density of soil (g/cm ³)	1.20	1.20
Density of soil particle (g/cm ³)	2.45	2.40
Permeability (cm/s)	5.75×10 ⁻³ (Sr=86.7%)	1.87×10 ⁻³ (Sr=89.1%)

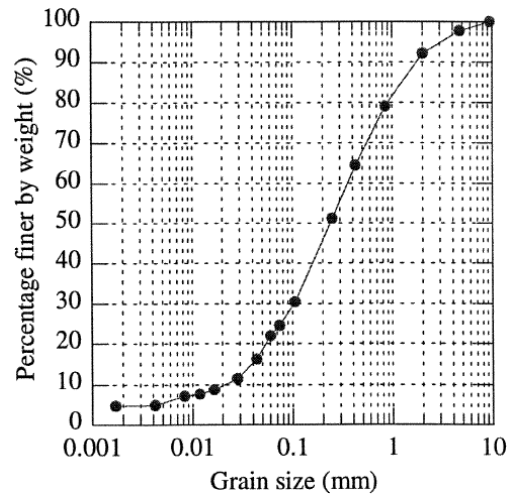
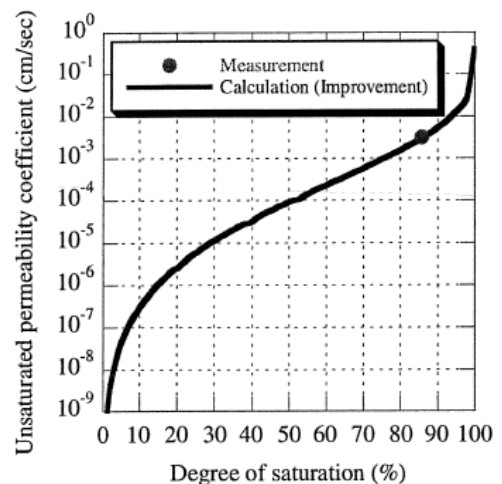
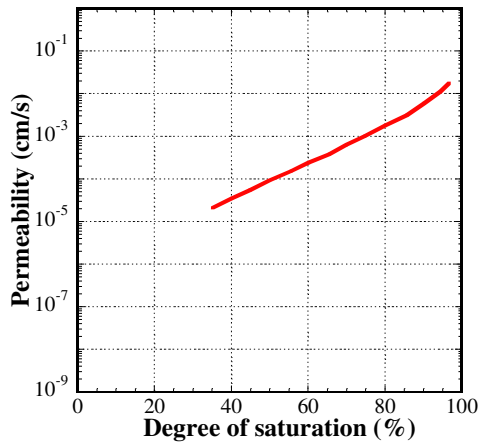


Figure 4 Grain size distribution of Shirasu (Sako *et al.*, 2006)

In the tests, in order to investigate the mechanism of slope failure, several patterns were carried out, among which two patterns were selected to be simulated by the proposed FE-FD analysis program. Figure 5(a) shows the relationship between permeability of unsaturated shirasu and the degree of saturation adopted in the work by Sako *et al.* (2006). In this study, the data of the permeability-saturation is the same as those Sako *et al.*, as shown in Figure 5(b). This relationship between the permeability and the saturation are well investigated and commonly accepted. The only thing need to do is to identify the order at one point. That is why only one point in Figure 5 (a) is plotted.



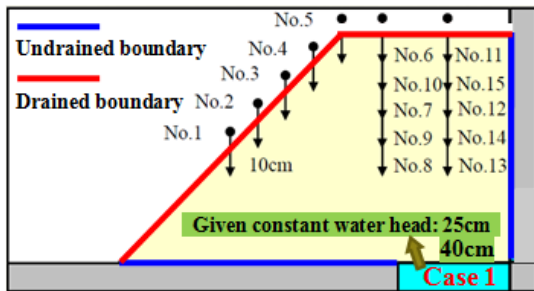
(a) Permeability-saturation relation (Sako *et al.*, 2006)



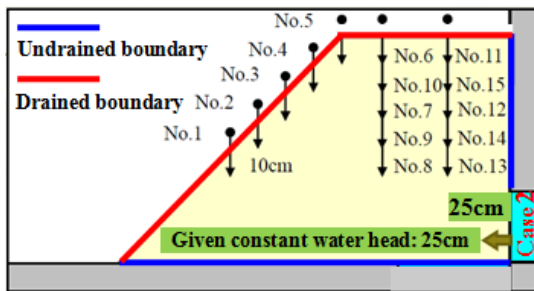
(b) Permeability-saturation relation used in calculation

Figure 5 Relationship between permeability and degree of saturation for unsaturated soil

Figure 6 shows the cross section of soil tank which has 180cm in length and 90 cm in depth. For the measuring devices, Tensiometers with a diameter of 18mm were used to measure negative pore water pressure and set at the depths of 10 cm, 20 cm, 30 cm, 40 cm and 50 cm, respectively on the slope. At the same time, the boundary conditions are also shown in Figure 6 for two cases. In Case 1, a constant water head of 25 cm is given at the bottom edge; while in Case 2, a constant water head of 25 cm is given at the side edge. In the figure, red line denotes drained boundary, blue line indicates undrained boundary.



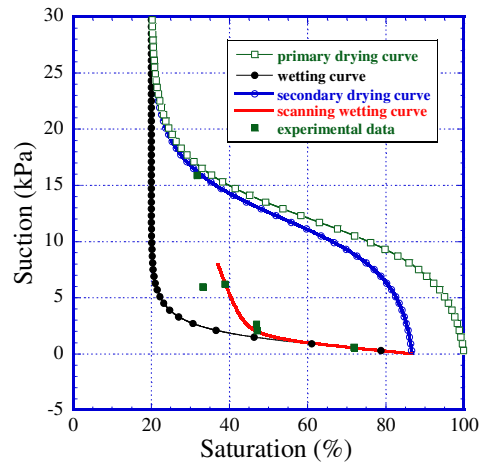
(a) Case 1



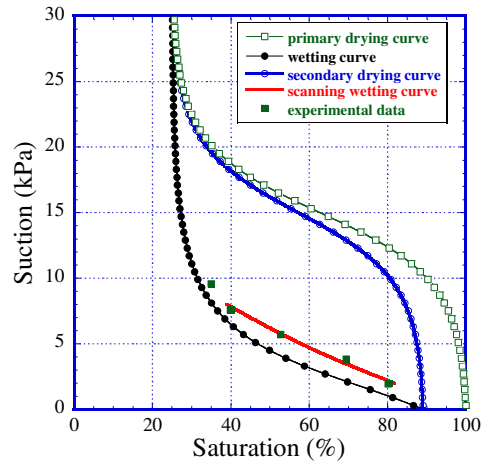
(b) Case 2

Figure 6 Layout of measurement and hydraulic condition in model tests

Figure 7 shows the moisture characteristics curves (MCC) indicated by square dots, which are obtained from the pressure plate method in the tests. From the test results, it is found out that the initial suction for two cases are around 8.0 kPa. The simulated MCC, calculated by the proposed MCC model, are also shown in the figures. It is known that the calculated MCC agrees well with the moisture characteristic observed in the tests. The parameters involved in the model are shown in Table 4.



(a) Case 1



(b) Case 2

Figure 7 Moisture hysteresis: test and simulation

Table 4 Parameters of MCC for unsaturated shirasu

	Case 1	Case 2
Saturated degrees of saturation S_r^s	0.867	0.891
Residual degrees of saturation S_r^r	0.200	0.250
Parameter corresponding to drying AEV (kPa) S_d	12	15
Parameter corresponding to wetting AEV (kPa) S_w	0.07	0.010
Initial stiffness of scanning curve (kPa) k_{sp}^c	90	20
Parameter of shape function c_1	0.30	0.30
Parameter of shape function c_2	0.60	0.20
Parameter of shape function c_3	30.0	10.0

Figure 8 shows 2D FEM mesh used in the simulation, with 1600 4-node isoparametric elements. The boundary condition is also shown in the figure. Table 5 lists the material parameters involved in the proposed model Apart from the void ratios at the normal consolidated line for saturated and unsaturated state ($N.C.L.S$) at a reference mean stress, other parameters are the same in two cases. The triaxial compression simulations of Shirasu under drained and exhausted conditions under different suctions are shown in Figure 9.

In the calculation, the initial stress field is a gravitational stress field and the initial suction is assumed to be uniformly distributed with a value of 8 kPa, which is exactly the same as the test condition (Kitamura *et al.*, 2007).

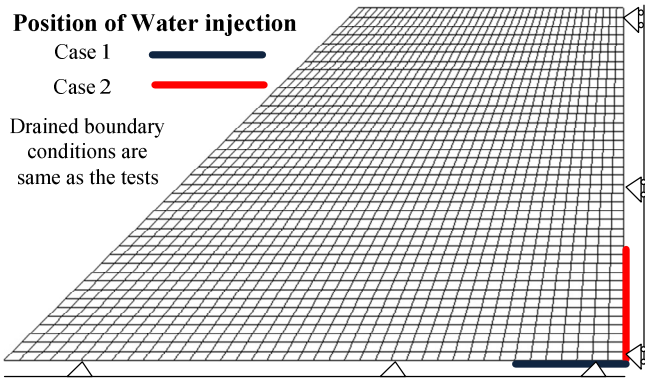


Figure 8 FEM mesh and boundary conditions

Table 5 Material parameters of unsaturated shirasu

	Case 1	Case 2
Compression index λ	0.055	0.055
Swelling index κ	0.01	0.01
Critical state parameter M	1.0	1.0
Void ratio N ($p'=98$ kPa on <i>N.C.L.</i>)	1.55	1.45
Poisson's ratio ν	0.30	0.30
Parameter of over consolidation a	2.0	2.0
Parameter of suction b	0.5	0.5
Parameter of over consolidation	1.0	1.0
Void ratio N_r ($p'=98$ kPa on <i>N.C.L.S.</i>)	1.57	1.47

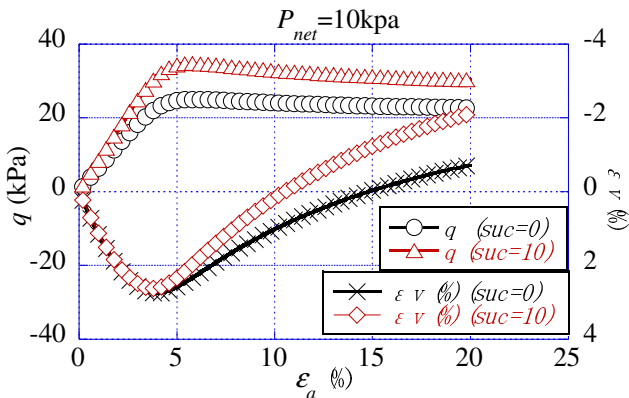


Figure 9 Triaxial compression simulation of Shirasu

Figure 10 shows the distributions of the degree of saturation at specified times for Case 1 and Case 2 respectively. From these figures, it is seen that the water is infiltrating toward slope surface from the initial position with time for both cases. 300 min after the start of water infiltration, the water had reached the toe of slope in Case 1. While in Case 2, the water had not reached the toe.

Figure 11 shows the contours of plastic shear strain $\sqrt{2I_2^p}$ at different times in both cases. Here, I_2^p is the second invariant of deviatoric plastic strain tensor. From these figures, it is easy to know that a concentrated plastic shear zone firstly occurred at the area near the slope surface in both cases due to water seepage. After then a shear band formed within the slope at about 260min in Case 1. In Case 2, however, the shear band did not occur at all.

Figure 12 shows the changes of displacement vectors with time for Cases 1 and 2, respectively. For both cases, the ground surface near back side moves downward on the whole at first 100 min due to water seepage. After then the ground above the shear band in Case 1 moved towards the toe while the other ground almost kept unmoved. It can be seen that there is a clear slip area along the shear

band at time 300 min. In Case 2, however, such slip behavior did not show up.

Based on the results shown in Figures 10, 11 and 12, it is reasonable to judge that the slope is much more danger in Case 1 than in Case 2, which is consistent with the test results in which an entire slope failure had happened in Case 1.

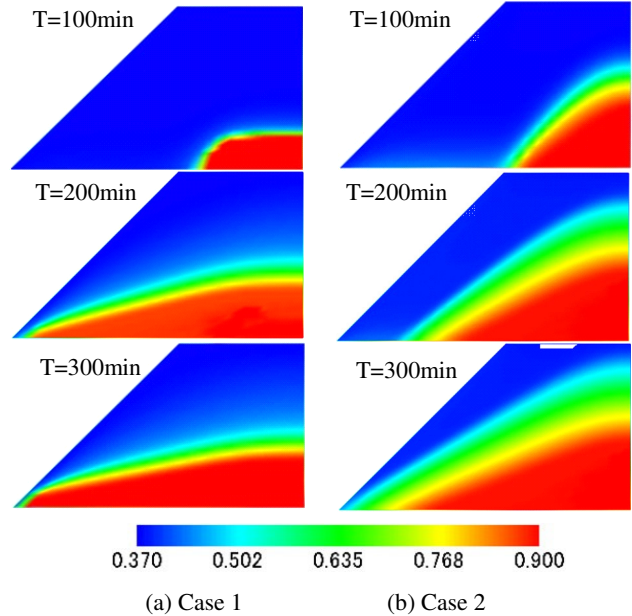


Figure 10 Distribution of saturation at specific times

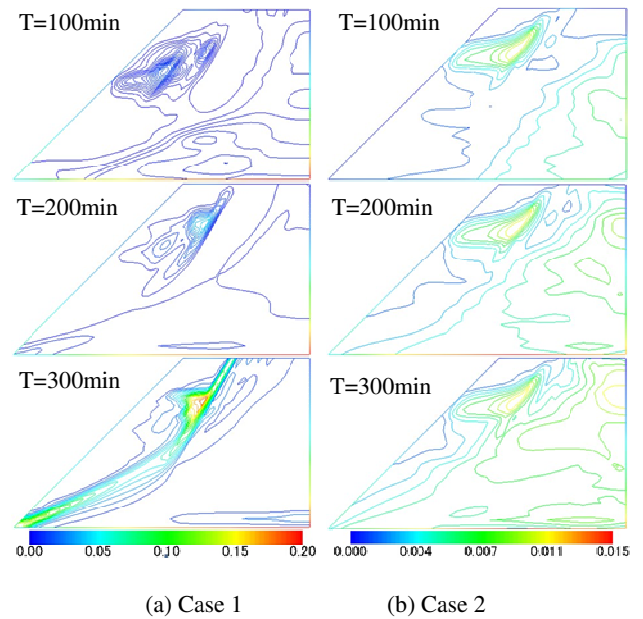


Figure 11 Contours of plastic shear strain ($\sqrt{2I_2^p}$)

Figures 13 and 14 show the comparisons of the development of pore water pressure (suction) at some measured points between the test and the simulated results In Case 1 and Case 2 respectively. From these figures, it is found out that the simulation can generally describe the development of pore water pressure quite well in the points far away from the slope surface. In the points along the slope surface, however, a rather big difference between the calculation and the test existed. This might be caused by the assumption that the coefficients of permeability are the same in vertical and horizontal direction, and that the initial suction is the same in whole model ground.

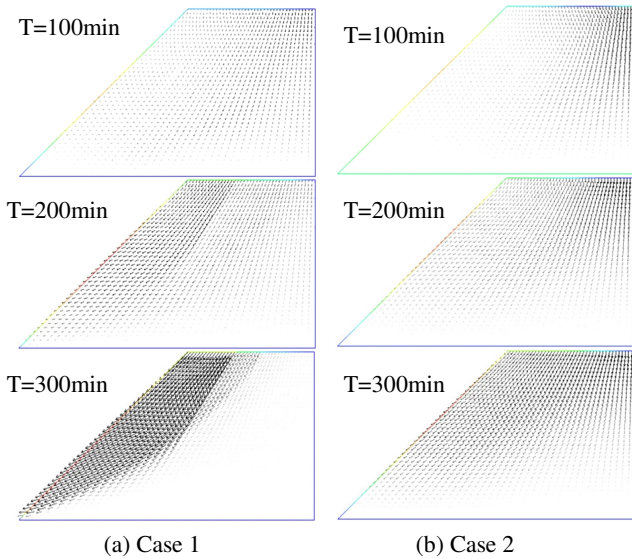


Figure 12 Development of displacement vector with time (Calculated maximum displacement = 13cm)

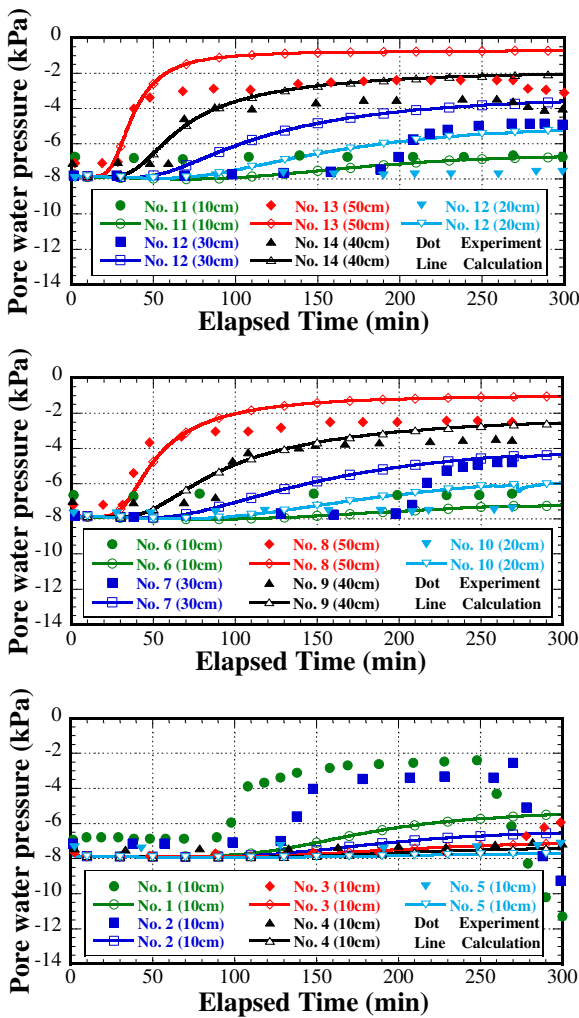


Figure 13 Development of pore water pressure with time (Case 1)

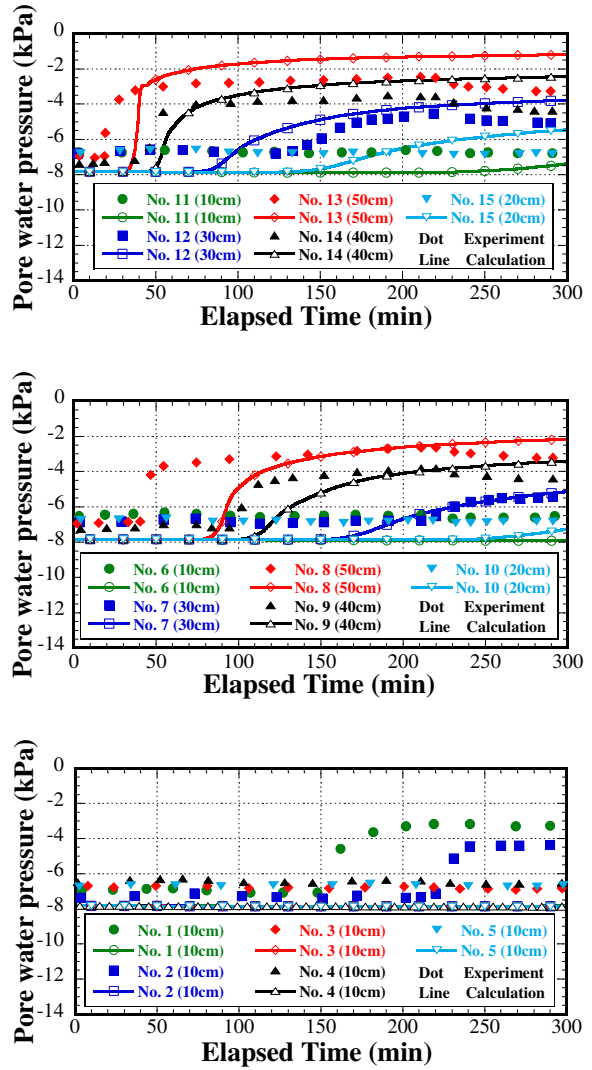


Figure 14 Development of pore water pressure with time (Case 2)

4. CONCLUSION

In this paper, a model test on slope failure (Kitamura *et al.*, 2007) is simulated by the proposed FE-FD program based on a rational elastoplastic model for unsaturated soil. The following conclusions can be made:

1. The field governing equations in soil-water-air three-phase problems are discretized in detail in FEM scheme with a proper incorporation of the constitutive model in which the degree of the saturation is taken as the state variable.
2. The simulation of an element subjected to different loading and water infiltration has been conducted as a boundary value problem and it is known that the collapse behavior due to the increase of degree of saturation commonly observed in water infiltration test can be well described by the proposed numerical analysis.
3. The model tests on slope failure due to suction reduction have been simulated. It is known from the comparison between the test and calculated results that the seepage-deformation coupled behavior of unsaturated soil ground can be well described by the proposed analysis.

5. REFERENCES

- Borja R. (2005) "Conservation laws for three-phase partially saturated granular media", *Unsaturated Soils: Numerical and Theoretical Approaches*, 94, pp 3-14.
- Kitamura R. *et al.* (2007) "Soil tank test on seepage and failure behaviors of Shirasu slope during rainfall", *Japanese Geotechnical Journal*, 2(3), pp 149-168 (in Japanese).
- Li C, Borja R. and Regueiro R. (2004) "Dynamics of porous media at finite strain", *Computer Methods in Applied Mechanics and Engineering*, 193, pp 3837-3870.
- Oka F., Yashima A. and Shimata T. (1994) "FEM-FDM coupled liquefaction analysis of a porous soils using an elasto-plastic model", *Applied Scientific Research*, 52, pp 209-245.
- Sako K., Kitamura R. and Fukugawa R. (2006) "Study of slope failure due to rainfall: a comparison between experiment and simulation", *Proc. of 4th International Conference on Unsaturated Soil*, 2, pp 2324-2335.
- Tohari A., Nishigaki M. and Komutsu M. (2007) "Laboratory rainfall-induced slope failure with moisture content measurement", *Journal of Geotechnical and Geoenvironmental engineering*, 133(5), pp 575-587.
- Uzuoka *et al.* (2007) "Finite element analysis for dynamic finite deformation in unsaturated soil", *Proceedings of the conference on computational engineering and science*, 12(2), pp 523-526 (in Japanese).
- Uzuoka *et al.* (2008) "Finite element analysis of coupled of unsaturated soil and water using aerial elements", *Proceedings of the Conference on Computational Engineering and Science*, 13(1), pp 219-222 (in Japanese).
- Uzuoka *et al.* (2009) "Soil-water-air coupled dynamic analysis of unsaturated fill", *Proceedings of the Conference on Computational Engineering and Science*, 14(1), pp 461-464 (in Japanese)
- Uzuoka R. (2010) "Effective stress analysis (Finite deformation scheme)", Private Discussion.
- Yaki N., Yatabe R. and Yamamoto K. (1983): "Slope failure due to seepage of rainwater", *Japanese Journal of Civil Engineering*, 330(2), pp 107-114.
- Zhang F. and Ikariya. T. (2011): "A new model for unsaturated soil using skeleton and degree of saturation as state variables", *Soils and Foundations*, 51(1), pp 67-81.